Redox Biology 38 (2021) 101794

Contents lists available at ScienceDirect

Redox Biology

journal homepage: www.elsevier.com/locate/redox

RAC1 nitration at Y^{32} IS involved in the endothelial barrier disruption associated with lipopolysaccharide-mediated acute lung injury

Ting Wang [a,1], Manivannan Yegambaram [b,1], Christine Gross [c,d], Xutong Sun [b], Qing Lu [b], Hui Wang [b], Xiaomin Wu [b], Archana Kangath [b], Haiyang Tang [b], Saurabh Aggarwal [d,e], Stephen M. Black [b,*]

[a] Department of Internal Medicine, College of Medicine Phoenix, University of Arizona, Phoenix, AZ, USA
[b] Division of Translational and Regenerative Medicine, Department of Medicine, College of Medicine Tucson, University of Arizona, Tucson, AZ, USA
[c] Department of Medicine at Broward Health Medical Center, Fort Lauderdale, Florida, USA
[d] Vascular Biology Center, Augusta University, Augusta, GA, Georgia
[e] Department of Anesthesiology and Perioperative Medicine and Division of Molecular and Translational Biomedicine, School of Medicine, University of Alabama at Birmingham, Birmingham, AL, USA

ARTICLE INFO

Keywords:
Rac1
Nitration
LPS
Acute lung injury

ABSTRACT

Acute lung injury (ALI), a devastating illness induced by systemic inflammation e.g., sepsis or local lung inflammation e.g., COVID-19 mediated severe pneumonia, has an unacceptably high mortality and has no effective therapy. ALI is associated with increased pulmonary microvascular hyperpermeability and alveolar flooding. The small Rho GTPases, RhoA and Rac1 are central regulators of vascular permeability through cytoskeleton rearrangements. RhoA and Rac1 have opposing functional outcome: RhoA induces an endothelial contractile phenotype and barrier disruption, while Rac1 stabilizes endothelial junctions and increases barrier integrity. In ALI, RhoA activity is increased while Rac1 activity is reduced. We have shown that the activation of RhoA in lipopolysaccharide (LPS)-mediated ALI, is dependent, at least in part, on a single nitration event at tyrosine (Y)^{34}. Thus, the purpose of this study was to determine if the inhibition of Rac1 is also dependent on its nitration. Our data show that Rac1 inhibition by LPS is associated with its nitration that mass spectrometry identified as Y^{32}, within the switch I region adjacent to the nucleotide-binding site. Using a molecular modeling approach, we designed a nitration shielding peptide for Rac1, designated NipR2 (nitration inhibitor peptide for the Rho GTPases 2), which attenuated the LPS-induced nitration of Rac1 at Y^{32}, preserves Rac1 activity and attenuates the LPS-mediated disruption of the endothelial barrier in human lung microvascular endothelial cells (HLMVEC). Using a murine model of ALI induced by intratracheal installation of LPS we found that NipR2 successfully prevented Rac1 nitration and Rac1 inhibition, and more importantly attenuated pulmonary inflammation, reduced lung injury and prevented the loss of lung function. Together, our data identify a new post-translational mechanism of Rac1 inhibition through its nitration at Y^{32}. As NipR2 also reduces sepsis induced ALI in the mouse lung, we conclude that Rac1 nitration is a therapeutic target in ALI.

1. Introduction

The current pandemic of COVID-19 has caused over a hundred and sixty thousand deaths in USA, mainly due to a severe form of lung inflammation and edema, called acute lung injury (ALI) or its severe form acute respiratory distress syndrome (ARDS) [1]. ALI and ARDS represent the same disease spectrum characterized by hypoxemic respiratory insufficiency from pulmonary edema [2]. The acute lung inflammation and increased vascular hyperpermeability associated with ALI can be caused by systemic inflammation such as sepsis, or lung inflammation such as severe pneumonia induced by COVID-19 or other bacteria or viruses [3]. Besides supportive care with low tidal volume mechanical ventilation, general anti-inflammatory steroids, and extra-corporeal membrane oxygenation (ECMO) in the intensive care unit

* Corresponding author.Division of Translational and Regenerative Medicine, Department of Medicine, The University of Arizona Health Sciences, Tucson, AZ, 85724, USA.
E-mail address: steveblack@email.arizona.edu (S.M. Black).
[1] contributed equally to the study.

https://doi.org/10.1016/j.redox.2020.101794
Received 19 September 2020; Received in revised form 6 November 2020; Accepted 7 November 2020
Available online 13 November 2020

(ICU), there are no specific drug therapies for ALI/ARDS, which still has an unacceptably high mortality of ~30% [4]. Thus, a devastating demand for effective therapies for ALI/ARDS exists.

A leading cause of ALI/ARDS is the excessive release of endotoxin or lipopolysaccharide (LPS) from the outer membrane of gram-negative bacteria, during sepsis [5]. The subsequent disruption of the microvascular capillary integrity leads to endothelial hyperpermeability and alveolar flooding. This leads to an accumulation of protein rich fluid in the alveolar space, impairing gas exchange, and precipitating respiratory distress [1]. LPS-mediated vascular bed integrity disruption is complex, although oxidative and nitrative stress is one of the leading pathobiological mechanisms associated with endothelial barrier disruption [6]. LPS induces overproduction of nitric oxide (NO) and superoxide in endothelial cells. These two hyper-reactive radicals form peroxynitrite and subsequently protein nitration [7,8]. Cellular protein nitration, similar to phosphorylation, can alter the structure and function of specific proteins, through its interaction with the aromatic ring of tyrosine residues [9]. Extensive evidence suggests that protein nitration is implicated in the pathogenesis of a number of diseases [10–13]. In a murine model of LPS induced acute lung injury, we have previously shown that a peroxynitrite scavenging strategy decreases lung edema, implicating protein nitration in the progression of ALI [8].

Endothelial barrier regulation is dependent on cytoskeleton rearrangements [14]. The small GTPases of the Rho protein family, RhoA, Rac1 and Cdc42 are key regulators of the actin cytoskeleton [15]. Rac1 and RhoA have antagonistic effects on endothelial barrier function in the lung [16,17]. RhoA destabilizes endothelial junctions by increasing myosin driven contractility via myosin light chain phosphatase inhibition, while Rac1 facilitates the assembly and maintenance of endothelial adherens junctions [18]. Disruption of the balance between RhoA and Rac1 signaling leads to several human pathologies including ALI/ARDS. We reported earlier that LPS-induced peroxynitrite generation leads to RhoA nitration and activation [19], however nothing is known about possible nitration-mediated post-translational regulation of its endogenous counter, Rac1, a protein sharing significant similarities in structure and function. Using a systems-biology like approach (protein modification→cellular function→disease modulation→therapeutic strategy design), we investigated whether Rac1 activity was also regulated by protein nitration. For the first time, we were able to show that LPS induces Rac1 nitration and this is directly associated with an inhibition of its activity. Further, we were able to demonstrate that Rac1 nitration is a key regulator of endothelial barrier disruption during sepsis, especially during the recovery phase. We identified the specific nitration site (Y^{32}), and designed a peptide, NipR2, which binds to the nitration site and shields Y^{32} from nitration by peroxynitrite. We were able to demonstrate that this shielding peptide is protective against LPS-induced Rac1 nitration, pulmonary vascular leakage, lung injury and the loss of lung function associated with LPS challenge in the mouse lung.

2. Materials & methods

2.1. Cells and reagents

Human lung microvascular endothelial cells (HLMVEC) were isolated and cultured as described previously [20]. Primary antibodies used in this project were purchased from Cell Signaling and Sigma-Aldrich (Rac1 antibody), Calbiochem and Cell Signaling (3-Nitrotyrosine), and Sigma-Aldrich (β-actin). The Rac1 GTPase activity kit was purchased from Cytoskeleton. LPS, SIN1, peroxynitrite and MnTMPyP were purchased from Sigma-Aldrich. Other biochemicals and chemicals were purchased from Sigma-Aldrich unless specifically stated.

2.2. Cell experiments

HLMVEC were challenged with LPS (1 EU/ml, 4 h) in the presence or absence of the peroxynitrite scavenger, MnTMPyP (25 μM). In other sets of experiments, cultured HLMVEC were pretreated with either NipR2 or NipR2F (5 μM, 5min) prior to LPS challenge (1 EU/ml, 4 h).

2.3. Western blot analysis

HLMVEC and mouse lung tissues were lysed using the protocol previously described [21,22]. Total cell lysate protein concentrations were calculated using BCA protein assay kit (Thermo-Fisher). Cell lysates with equal amount of protein were separated on 12% gels (Bio--Rad) and transferred to PVDF membrane (Bio-Rad), then blocked with 5% nonfat dry milk in Tris-buffered saline, 0.1% Tween 20 (TBST). The membranes were probed with respective primary antibody in blocking buffer, and the secondary antibody in blocking buffer after three time of wash in TBST. Reactive bands were visualized using chemiluminescence (Pierce) using either a Kodak 440CF image station or a LI-COR Biosciences Odyssey Imaging System. Band intensity was quantified using either Kodak 1D image processing software or Image Studio software version 5.

2.4. Immunoprecipitation analysis

HLMVEC were homogenized in Pierce IP lysis buffer (Thermo-Fisher). After centrifugation, the supernatant was collected and mixed with A/G agarose beads (EMD/Calbiochem) with the pull-down antibody for 2 h at 4 °C. The beads were collected after centrifugation at 5000 rpm for 5 min and washed 3 times with IP wash buffer (Thermo-Fisher). The beads were then boiled with 2x Laemmli buffer for 5 min. Proteins were separated on 12% gels and transferred to PVDF membrane and analyzed using Western blot methods described above. In another experiment, immunoprecipitated proteins in gel stained with Coomassie blue dye were digested with chymotrypsin and used for mass spectrometry.

2.5. Analysis of Rac1 activity

Rac1 activity was measured using the Rac1 Pull-Down Activation Assay Biochem Kit (Cytoskeleton Inc.). Briefly, HLMVEC and mouse lung tissue were lysed using the cell lysis buffer and the lysate with PAK-PBD beads was incubated at 4 °C on a rotator for 1 h. The PAK-PBD beads were centrifuged at 5000 g and washed with wash buffer. Equal volume of 2x Laemmli sample buffer was added to each tube and boiled for 5 min. Samples were analyzed by SDS-PAGE and Western blot analysis as described above.

2.6. MALDI-TOF-TOF mass spectrometry

All spectra were taken on an AB Sciex 5800 MALDI-TOF-TOF mass spectrometer in positive reflector mode (10 kV) with a matrix of CHCA. Masses were calibrated to Sciex 6 peptides mix with their monoisotopic mass Bradykinin (2#9 clip) Angiotensin I (1296.6853) Glu1-Fibrinopeptide (1570.6774) ACTH (1#17 clip) (2093.0867) ACTH (18#39 clip) (2465.1989) ACTH (7#38 clip) (3657.9294). The human Rac1 protein was digested with chymotrypsin (overnight in-gel digestion, 30 °C) and cleaned with C18 ZipTip (Millipore). C18 bound peptides were desalted and then eluted with 2.5 μl of acidic acetonitrile (75% CH3CN, 0.1% TFA). The eluant was mixed with 2.5 μl of freshly prepared CHCA stock solution (20 mg/ml CHCA in 50% acetonitrile, 0.1% Trifluoroacetic acid), and 1 μl portions of this mixture were spotted onto the AB Sciex MALDI TOF sample plate for air-drying. MS/MS of peptides were performed in positive reflector mode with collision-induced dissociation. MS and MS/MS spectra were analyzed using ProteinPilot software 5.0.1 and Mascot Distiller package. To evaluate NipR2 peptide nitration, we exposed NipR2 to authentic peroxynitrite (100 μM) for 30 min. Samples were desalted using a C-18 ZipTip, mixed with CHCA matrix and were spotted directly onto a MALDI plate for further MS and MS/MS analysis. The ability of NipR2 or NipR2F peptides to

bind to Rac1 was also analyzed by mixing 100 ng/ml of peptide with 100 ng/ml of human recombinant Rac1 protein for 45 min at RT and using MALDI MS Linear mode acquisition with sinapinic acid as a matrix.

2.7. Molecular modeling

The Yet Another Scientific Artificial Reality Application (YASARA) computer program was used for molecular visualizing, modeling, and dynamics. Analysis of the x-ray crystal structure of Rac1 and RhoA proteins showed that their respective nitrated tyrosines (Y^{32} in Rac1 and Y^{34} in RhoA) are located in a flexible region (flap) of the Switch I domain responsible for nucleotide binding. Molecular modeling analysis of the flap region in Rac1 nitrated at Y^{32} was carried out and the movement of the flap region was superimposed onto the x-ray crystal structure of Rac1 protein. Similarly, molecular modeling analysis of the flap region in RhoA nitrated at Y^{34} was carried out and the movement of the flap region was superimposed onto the X-ray crystal structure of RhoA protein.

2.8. Generation of a nitration-specific Rac1 polyclonal antibody (Rac1-Y^{32}-NO2)

A nitro-Y^{32} Rac1 specific antibody (Rac1-Y^{32}-NO_2) was raised against a synthetic peptide antigen (LLISYTTNAFPGEY^{NO2}IPTVFD), where Y–NO_2 represents 3-nitrotyrosine as previously described [23]. The peptide was used to immunize rabbits. Tyrosine nitration-reactive rabbit antiserum was first purified by affinity chromatography. Further purification was carried out using immunodepletion using non-nitrated peptide (LLISYTTNAFPGEYIPTVFD) resin chromatography, after which the resulting eluate was tested for antibody specificity by immunoblotting and immunoprecipitation followed by mass spectrometry. The RhoA-Y^{34}-NO_2 antibody was generated as previously described [24].

2.9. Rac1 overexpression plasmid construction and protein purification

His-tagged Rac1 recombinant protein was expressed in *E. coli* as previously described [19]. Briefly, isopropyl-beta-D-thiogalactopyranoside (IPTG, 1 mM) was added and the cells were incubated for 18–20 h at 25 °C. Bacteria were then harvested by centrifugation and the pellet was immediately lysed in 40 mM Tris-HCl, 5% glycerol, 1 mg/ml lysozyme, 100 mM NaCl, protease inhibitor cocktail, ribonuclease A (Sigma), and deoxyribonuclease I (Sigma). The pellet was gently rocked for 30 min, sonicated and subjected to ultracentrifugation. The supernatant was loaded onto a Hisprep FF 16/10 column (Sigma) using binding buffer (40 mM Tris-HCl, 100 mM NaCl, 5% glycerol, 30 mM imidazole) at 0.1 ml/min flow. The column was washed with 40 mM Tris-HCl, 300 mM NaCl, 5% glycerol, 30 mM imidazole using a flow rate of 1.5 ml/min. Elution of the histidine-tagged protein was accomplished using elution buffer (40 mM Tris-HCl, 300 mM NaCl, 5% glycerol, 400 mM imidazole) at 1.0 ml/min flow. Collected fractions were loaded for size-exclusion gel filtration on a HiLoad 26/600 Superdex 75 column (Sigma) using gel filtration buffer (60 mM Tris-HCl, 100 mM NaCl, 5% glycerol) at 0.2 ml/min flow. Fractions were collected and analyzed by Coomassie blue staining and Western blot. All purification steps were performed at 4 °C, and purified protein was stored at -80 °C. Recombinant human RhoA protein was also purified using a bacterial expression system as previously described [19].

2.10. Adenoviral mediated Rac1 overexpression and protein purification

Pulmonary arterial endothelial cells (PAEC) were cultured as described [25]. Ovine PAEC, isolated as previously described [25], were transduced with a His-tagged Rac1 adenovirus (MOI = 5) and incubated for 48 h at 37 °C. Cells were lysed and the His-tagged Rac1 protein was purified using HisPur Ni-NTA Columns (Thermo Scientific) and stored at -80 °C. Fractions were analyzed by Coomassie blue staining and Western blot analysis.

2.11. Rac1 nitration shielding peptide synthesis

Peptides containing 10 amino acids (FPGEYIPTVF) from aa28-37 of Rac1 fused with the cell permeable TAT sequence were synthesized by Peptide 2.0 Inc (Chantilly, VA). This peptide was designated NipR2 (nitration inhibitory peptide for the Rho GTPases 2) and designed to interact with the flap region of the Rac1 protein. A similar phenylalanine-substituted peptide (NipR2F) was also synthesized harboring a Y32F mutation.

2.12. In vitro permeability assays

The electrical resistance of the endothelial cell monolayer was measured with the electrical cell impedance sensor (ECIS) technique [26]. HLMVEC were cultured on gold plated electrodes (8E10+) until 95% confluence. The change in electric resistance across the monolayer was measured continuously. The data was normalized to the initial values of basal resistance. In the transwell permeability assay, HLMVEC were seeded on a semi-permeable membrane in the upper chamber of the transwell (1 μm pore size, BD Biosciences, San Jose, CA). After appropriate treatments, 40,000 MW FITC-dextran (1 μg/μl) (Sigma-Aldrich) was added to the upper chamber. The amount of FITC-dextran infiltrating into the lower chamber was determined using a Fluoroskan Ascent Fluorometer.

2.13. Mouse models of acute lung injury (ALI)

The Committee on Animal Research at Georgia Regents University and University of Arizona approved all animal protocols and procedures. In the pre-injury model, male C57BI/6 mice (10 weeks) received vehicle (saline) or MnTMPyP (5 mg/kg body weight) via an intraperitoneal injection 30 min before intratracheal installation of *E. coli* 0127:B8 LPS, 6.75×10^4 Endotoxin Units/g body weight, Sigma-Aldrich). Mice were examined 12 h after LPS challenge. At the end of the treatment, animals were anesthetized, and the lungs were flushed with 3 ml of ice-cold PBS (to remove blood) gently, and excised. A portion of the lung was quickly snap-frozen in liquid nitrogen and stored at -80 °C. In the post-injury model, male C57BI/6 mice (7–8 weeks) received vehicle (0.9% saline) or *E. coli* 0127:B8 LPS (1.25 mg/kg body wt, Sigma-Aldrich) prepared in 0.9% saline via an intratracheal injection 4 days before administration of NipR2 or NipR2F peptide (intraperitoneal injection, 1 mg/kg). On Day 7 (post LPS) mice were euthanized, lungs were flushed with 3 ml of ice-cold PBS (to remove blood) gently, and excised. A portion of the lung was quickly snap-frozen in liquid nitrogen and stored at -80 °C. The remaining lung tissue was fixed in PBS buffered formalin for histology analysis.

Isolation of Bronchoalveolar Lavage Fluid (BALF).

BALF was obtained by instilling and withdrawing 1 ml of ice-cold HANKS buffer (Sigma) via a tracheal cannula. BAL fluid was then centrifuged 500 *g* for 10 min to collect pelleted cells. BAL cells were then resuspended in red cell lysis buffer (RCLB) for 15 s, centrifuged 500 *g* for 10 min to remove RCLB, and resuspended in 200 μl of PBS. Total cell count was then determined using a haemocytometer. Cell suspension (50 μl) was also separated by Cytospin centrifuge (Thermo-fisher) 600 g for 10 min onto glass slides. After air dry, the slides were stained with Dif-Quik staining (VWR) for differential cell count.

2.14. Histological analysis of the mouse lung

Lungs were inflated with 10% formalin under 15 cm H_2O pressure and immersed in the same solution before tissue processing into paraffin-embedded blocks and 4 μm sections were then cut stained with

H&E. Histopathological assessment was conducted by two researchers who were masked to treatment group. H&E stained sections were scored for the presence of neutrophil in the alveolar space, neutrophils in the interstitial space, the existence of hyaline membranes, proteinaceous debris filling the airspaces and alveolar septal thickening as described previously [27].

2.15. Analysis of lung function

Mice were remaining anesthetized with isoflurane (5% with oxygen), tracheostomized with a metal 1.2 mm (internal diameter) cannula and connected to a Flexi Vent (Scireq Inc) ventilator. Ventilation was initiated at a tidal volume of 10 ml/kg and a rate of 150/min. A TLC maneuver was performed, followed by 15 s later, by a sinusoidal 1 Hz oscillation. Subsequently, an 8 s forced oscillatory signal (0.5–19.6 Hz) was applied, the mechanical input impedance of the respiratory system was calculated, and a model containing a constant phase tissue compartment was fit to input impedance in order to evaluate tissue elastance. Dynamic pressure-volume maneuvers were performed by stepwise increasing the airway pressure to 30 cm H_2O and then reversing the process. Transcutaneous oxygen saturation were monitored via a small animal pulse oximeter (MouseOx Plus, STARR Life Sciences Corporation, Oakmont, PA, USA) by placing the non-invasive sensor on the neck, as previously described [28].

2.16. Statistical analysis

Statistical analysis was performed using GraphPad Prism version 4.01 (GraphPad). The mean ± SD or SEM was calculated for all samples, and the significance was determined either by the unpaired *t*-test (for 2 groups) and ANOVA (for ≥ 3 groups). For the ANOVA analyses, Newman-Kuels post-hoc testing was employed. A value of $P < 0.05$ was considered significant.

3. Results

LPS decreases Rac1 activity through the nitration of Tyrosine 32 (Y^{32}).

In cultured HLMVEC, LPS challenge (1 EU/ml) induced significant decrease in Rac1 GTPase activity and this was attenuated by the peroxynitrite scavenger, MnTMPyP (Fig. 1A). Utilizing immunoprecipitation analyses we demonstrated that Rac1 is subject to protein nitration and again this is attenuated by MnTMPyP (Fig. 1B&C). These findings suggest that LPS-mediated Rac1 nitration is associated with reduced Rac1 GTPase activity. To further confirm the nitration on Rac1 peptide and identify the nitration site, we first utilized recombinant human Rac1 protein purified using an expression purification system based in *E.coli* [19]. Purity of Rac1 was determined to be >90% using both SDS PAGE with Coomassie staining (Fig. 2A) and Western blot analysis (Fig. 2B). The purified recombinant human Rac1 protein was exposed to authentic peroxynitrite (100 μM, 30 min) and then digested using chymotrypsin endoproteinase. The resulting peptide fragments were subjected to MALDI-TOF MS and MS/MS analysis. A nitrated peptide (1044.4Da) with sequence TTNAFPGEY^{32} was identified with a single nitration site present on the tyrosine residue. A MS peak with +45Da in molecular weight difference (equal to nitro group addition) was observed with the nitrated Rac1 peptide fragment, within the region of aa24-32 (Fig. 2C). Further MS-MS analysis confirmed the peptide sequence and the position of the nitro-group as Y^{32} (Fig. 2C). We next investigated the nitration of Rac1 in cultured pulmonary arterial endothelial cells (PAEC). In order to achieve a quantifiable intracellular level of Rac1, PAEC were transduced with an adenovirus construct containing a His-tagged human wildtype Rac1. We confirmed that human Rac1 protein could be purified utilizing a HisPur Ni-NTA Column (Fig. 2D). Rac1 purification was confirmed by SDS PAGE with Coomassie staining (Fig. 2D) and the identification of a single band by Western blot analysis (Fig. 2E). Transduced PAEC were then exposed to the peroxynitrite donor, SIN-1 (200 μM for 1 h) and Western blot analysis utilized to confirm that peroxynitrite did not alter total Rac1 levels in the cells (Fig. 2F). However, utilizing a nitrotyrosine antibody which specifically binds nitrated tyrosine we were able to see a strong band in Western blot at 21.5 kDa indicating a nitrated Rac1 protein in transduced PAEC exposed to SIN-1 (Fig. 2G). The nitrated Rac1 protein was then purified using HisPur Ni-NTA Column and the peptide fragments generated by overnight chymotrypsin digestion were subjected to MALDI-TOF MS and MS/MS analysis. After exposure to SIN-1, the same nitration site Y^{32} was detected in the Rac1 protein isolated from PAEC (Fig. 2H). These results indicate that peroxynitrite is capable of inducing Rac1 nitration at a specific site, Y^{32} both *in vitro* and *in vivo*. Next, using the known Rac1 protein structure and a previously established computational modeling

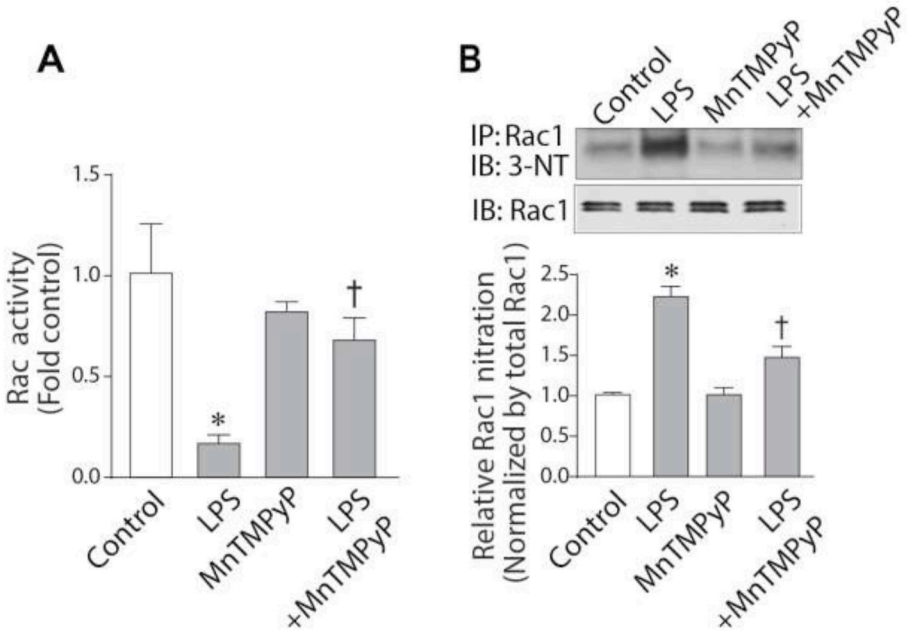

Fig. 1. LPS induces Rac1 nitration in endothelial cells. HLMVEC were challenged with LPS (1 EU/ml, 4 h) in the presence or absence of the peroxynitrite scavenger, MnTMPyP (25 μM). LPS attenuates Rac1 GTPAse activity and this is attenuated in the presence of MnTMPyP (A). Cell lysates were prepared for immunoprecipitation (IP) using an anti-Rac1 antibody followed by immunoblotting (IB) with an anti-3-Nitrotyrosine antibody (3-NT). Loading was normalized by reprobing the membranes with anti-Rac1. LPS increases Rac1 nitration and this is attenuated in the presence of MnTMPyP (B). Data are mean ± SEM. N = 4. *P < 0.05 vs. Control; †P < 0.05 vs. LPS alone.

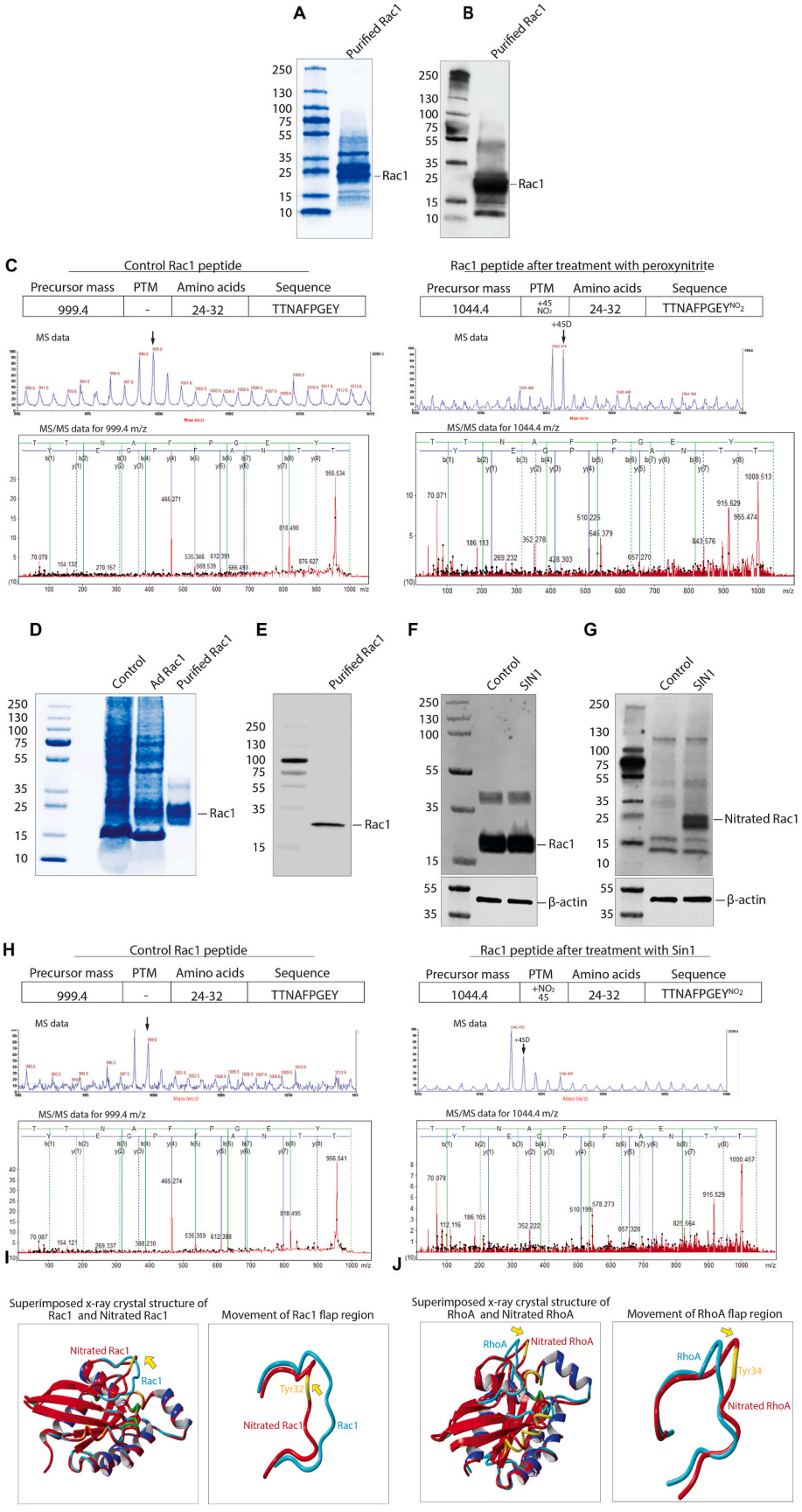

Fig. 2. Identification of Rac1 nitration site as Tyrosine (Y)[32].

method [19], we simulated the structural impact of Y^{32} nitration on Rac1. This modeling predicts that the Y^{32} containing region (the "flap" next to the Switch I region of the catalytic domain) leads to a "close" state in the flap region (Fig. 2I), compared to the "open" state induced by nitration of Y^{34} in the flap region of RhoA [19] (Fig. 2J). These computational modeling data, coupled with our Rac1-GTPase activity measurements (Fig. 1A), clearly demonstrate that LPS-mediated peroxynitrite stress induces Rac1 nitration at Y^{32} and that this is inhibitory for Rac1 GTPase activity.

3.1. LPS induces Rac1 nitration in the mouse lung

In order to increase the detection sensitivity for Y^{32} nitrated Rac1, we next generated a polyclonal antibody (Rac1-Y^{32}-NO_2) that specifically recognizes Y^{32} nitrated Rac1 following the protocol from the previous study which used an antibody (RhoA-Y^{34}-NO_2) that recognized Y^{34} nitrated RhoA [24]. We confirmed that the Rac1-Y^{32}-NO_2 antibody selectively detects Y^{32} nitrated Rac1 in recombinant protein exposed to authentic peroxynitrite *in-vitro* (Fig. 3A) and *in-vivo* HLMVEC exposed to SIN-1 (Fig. 3B). Further, we validated that Rac1-Y^{32}-NO_2 and RhoA-Y^{34}-NO_2 antibodies are preferential for nitrated Rac1 and nitrated RhoA respectively (Fig. 3C). Using Rac1-Y^{32}-NO_2 antibody we were next able to confirm that there was significant increase in Rac1 nitration in the mouse lung 12 h after I.T. LPS challenge, and that again Rac1 nitration was significantly suppressed by MnTMPyP (Fig. 3D). These changes in Rac1 nitration correlated with change in Rac1 GTPase activity (Fig. 3E). These data demonstrate that nitration of Rac1 at Y^{32}, is intimately involved in the loss of Rac1 activity in the mouse lung during sepsis-mediated ALI.

3.2. Generation and analysis of a Rac1 nitration shielding peptide

We next aimed to design a peptide which specifically targets the flap region of the Rac1 protein to prevent its nitration at Y^{32}. Docking simulations (Fig. 4A) were used to design a nitration shielding approach that would bind to the flaps region of Rac1 similar to that used earlier for RhoA [19]. This resulted in the design of a peptide with sequence HRKKRRQRRRQFPGEYIPTVF designated nitration inhibitory peptide for Rho GTPases 2 (NipR2). The molecular mass of the NipR2 peptide of 2755.5 Da was confirmed by MALDI MS (Fig. 4B) and peptide sequence was confirmed by MS/MS (Fig. 4C). The NipR2 peptide was then exposed to authentic peroxynitrite (100 μM, 30 min). MS and MS/MS analysis confirmed that this produced a +45 Da mass shift (2800.5 Da) related to the addition of a NO_2 group to the Tyrosine residue (Fig. 4B and C). Further, MS analysis of the nitrated NipR2 peptide revealed a photochemical decomposition pattern ([M+H]+, [M + H-16]+ and [M + H-32]+ (Fig. 4B). In another experiment, a control peptide (HRKKRRQRRRQFPGEFIPTVF) in which Y^{32} was substituted with a phenylalanine residue (NipR2F) was also synthesized. The molecular mass of the NipR2F peptide was confirmed as 2739.5 Da with MALDI MS (Fig. 4D) and peptide sequence was confirmed by MS/MS (Fig. 4E). As expected, when the NipR2F peptide was exposed to peroxynitrite (100 μM, 30 min) there was no mass difference observed in MS and MS/MS spectrum because of absence of the target tyrosine residue required for nitration (Fig. 4D and E). Using MALDI MS Linear mode acquisition, with sinapinic acid as a matrix, we also confirmed that both NipR2 and NipR2F peptides we able to bind efficiently to intact human recombinant Rac1 (Fig. 4F).

NipR2 peptide protects Rac1 from LPS-induced Rac1 nitration and inhibition in human lung microvascular endothelial cells.

HLMVEC were challenged with LPS (1 EU/ml, 4 h) and Rac1 protein was then immunoprecipitated and subjected to overnight in-gel chymotrypsin digestion. Similar to our earlier findings, a nitrated peptide with sequence TTNAFPGEY[32] was identified with a single nitration site present on the tyrosine residue. The MALDI MS also showed a photodecomposition pattern of the nitro group ([M+H]+, [M + H-16]+ and [M + H-32]+) (Fig. 5A). The MS/MS spectrum was analyzed using the Mascot Distiller package which identified the peptide sequence as TTNAFPGEY from a human Rac1 protein modified at Tyr^{32} by nitro group (Fig. 5A). Next, we utilized NipR2 (5 μM, 5 min before LPS challenge) to examine effects on Rac1 nitration and Rac1 GTPase activity in LPS challenged HLMVEC. Our data demonstrate that NipR2 pretreatment significantly attenuated LPS-induced Rac1 nitration (Fig. 5B) and preserved Rac1 GTPase activity (Fig. 5C) in HLMVEC. Conversely, NipR2F failed to block Rac1 nitration (Fig. 5D) or preserve Rac1 GTPase activity (Fig. 5E) in LPS challenged HLMVEC. NipR2 also successfully attenuated the LPS-mediated disruption of the HLMVEC barrier as determined both by preservation of transendothelial electrical resistance (Fig. 5F) and a reduction in transwell permeability of FITC-dextran (Fig. 5G). As expected, the NipR2F did not exhibit any functional activity upon LPS-mediated endothelial integrity loss (Fig. 5F&G). Together these data demonstrate that NipR2 can effectively attenuate Rac1 nitration, Rac1 activity inhibition, and endothelial barrier disruption in a cell model of LPS induced ALI.

NipR2 peptide attenuates Rac1 nitration and inhibition in the lungs of LPS treated mice.

To evaluate the therapeutic potential of NipR2, we utilized a mouse model of ALI induced by the intratracheal (i.t.) installation of LPS. Mice were challenged with LPS (1.25 mg/kg) and treated with NipR2 or NipR2F peptides (0.1 mg/kg) 4 days post LPS challenge and harvested 7 days post LPS challenge (Fig. 6A). As expected, NipR2, but not NipR2F, significantly attenuated LPS-mediated Rac1 nitration (Fig. 6B) and restored Rac1 GTPase activity (Fig. 6C). Mice were also used to perform additional physiological, biochemical and morphological studies to evaluate the efficacy of the NipR2 peptide in attenuating symptoms of ALI. Cell infiltration into the BALF was significantly increased in LPS treated animals (Fig. 6D). NipR2, but not NipR2F, reduced this increase (Fig. 6D). We also assessed histopathological changes in the lungs. LPS induces severe alveolar damage that includes the presence of large numbers of neutrophils and red blood cells in the alveolar and interstitial space, formation of hyaline membranes, septal thickening and debris accumulation in the alveoli (Fig. 6E). Again, NipR2, but not NipR2F, reduced these pathological changes (Fig. 6E &F).

3.3. NipR2 peptide preserves lung function in LPS treated mice

We next assessed the effect of NipR2 on lung function in LPS challenged mice. NipR2 restored oxygen saturation from ~72% to ~95% (Fig. 7A). Using FlexiVent technology, we also performed respiratory pressure-volume loop (PV loop) measurement and analysis. LPS induced a characteristic downward shift of the PV loop, compared to control mice (Fig. 7B). Consistent with the oxygen saturation findings, NipR2, but not NipR2F, restored the PV loop, indicative of an improvement in respiratory mechanical function. Specifically, NipR2 increased the respiratory maximal volume at highest pressure (Fig. 7C). NipR2 also prevented the LPS-mediated attenuation of total respiratory compliance (Fig. 7D) and the increase in respiratory elastance (Fig. 7E). Together these data demonstrate that NipR2 significantly improved lung function in this murine model of acute lung injury.

4. Discussion

ALI is a complex syndrome with an unacceptable mortality. ALI pathogenesis involves disruption of the epithelial and endothelial barriers leading to an increased permeability and decreased edema fluid clearance [29]. Lung barrier permeability is tightly regulated by adherens junctions, tight junctions, and gap junctions. Junctional integrity is vital for cell-cell adhesion, actin cytoskeleton remodeling, intercellular signaling, and transcriptional regulation [30]. Rac1 regulates lung endothelial integrity via cytoskeleton rearrangements that determine cell shape and junctional integrity of the lumen [31]. Interestingly, within the Rho-family small GTPases, Rac1 and RhoA are antagomirs

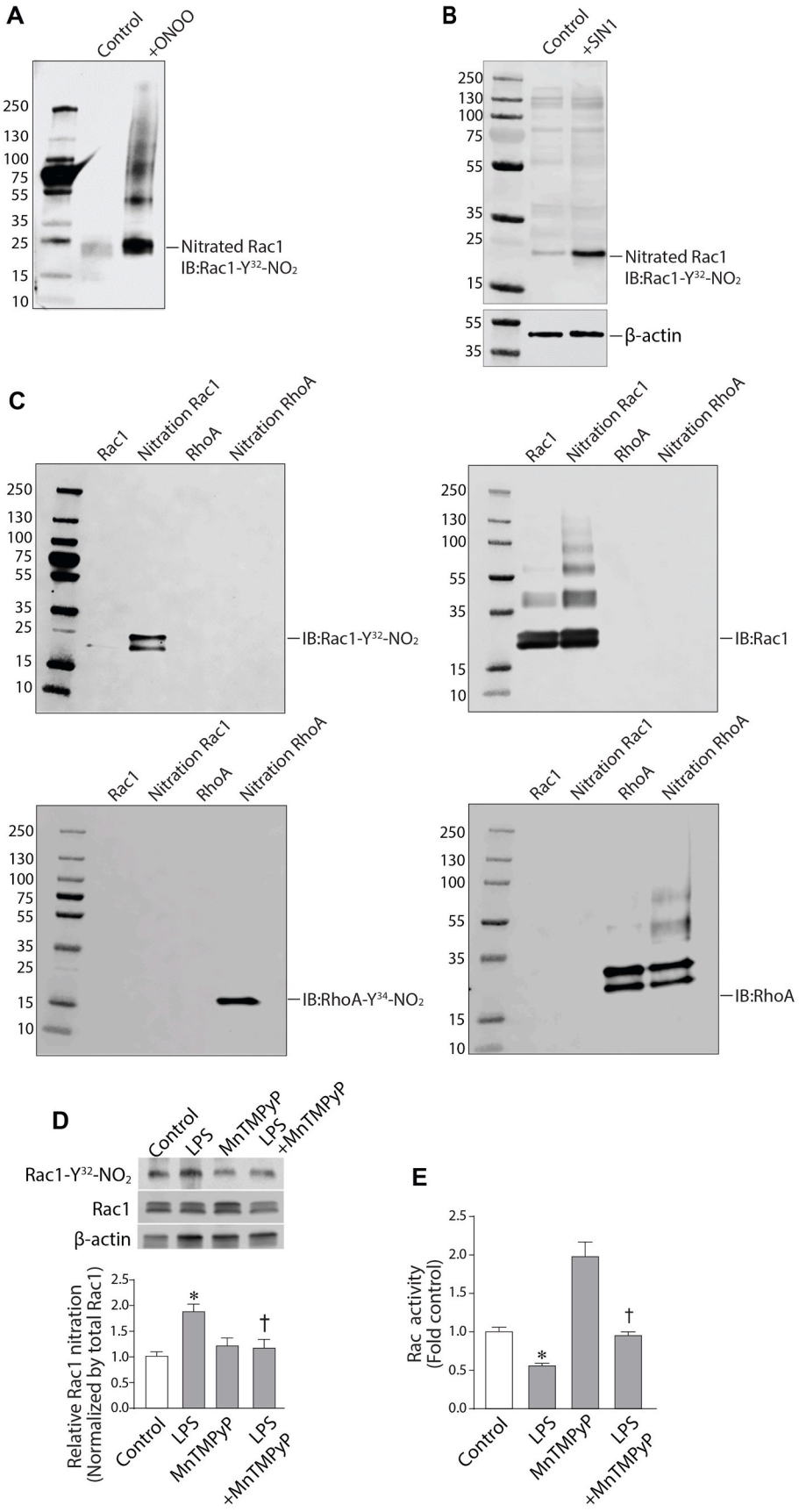

Fig. 3. LPS induces Rac1 nitration in the mouse lung.

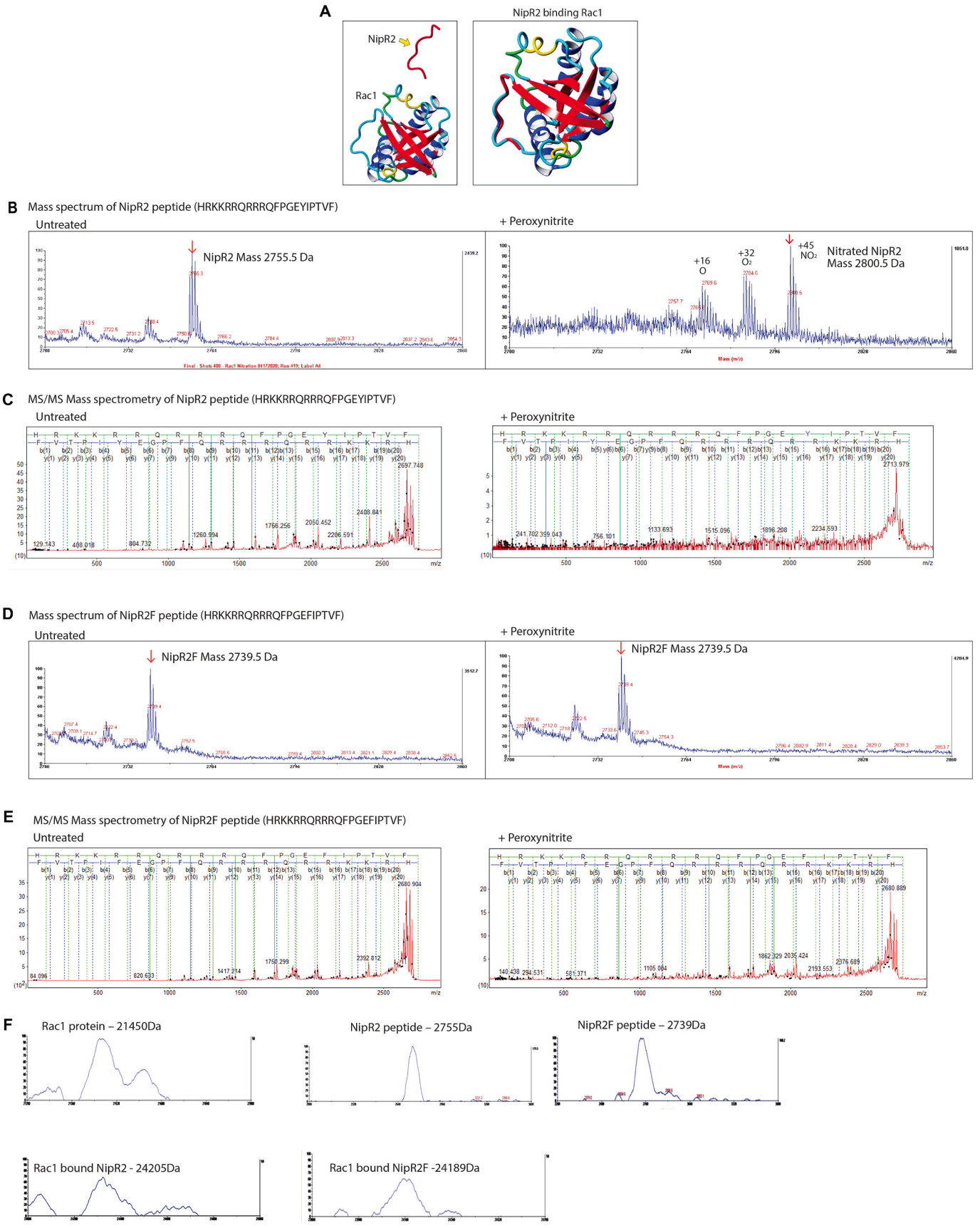

(caption on next page)

Fig. 4. Development of a nitration shielding peptide for Rac1 to prevent Y^{32} nitration. Molecular modeling analysis shows the interaction between the peptide sequence FPGEYIPTVF and the flap region of Rac1 protein (A). This sequence was fused with the cell permeable TAT sequence to produce NipR2 (HRKKRRQRRRQFPGEYIPTVF). The NipR2 peptide mass was confirmed by MALDI-MS to have a molecular weight of 2755.5 Da. Exposure of NipR2 to peroxynitrite (100 μM, 30 min) produced a +45 Da mass shift (2800.5 Da) produced by NO_2 group addition to the tyrosine residue (HRKKRRQRRRQFPGEY^{NO2}IPTVF) (B). MS/MS analysis of the NipR2 peptide (2755.5 Da) and nitrated NipR2 peptide (2800.5 Da) after treatment with peroxynitrite were obtained in positive reflector mode. MS/MS analysis confirmed the change in peptide mass after exposure of NipR2 to peroxynitrite (C). A control peptide was also produced in which the tyrosine residue was replaced by a phenylalanine to produce NiPR2F (HRKKRRQRRRQFPGEFIPTVF). Exposure of NipR2F to peroxynitrite (100 μM, 30 min) caused no change in molecular weight (2739.5 Da) (D). MS/MS analysis of the NipR2F peptide (2739.5 Da) and NipR2F peptide after treatment with peroxynitrite were obtained in positive reflector mode. MS/MS analysis confirmed no change in peptide mass after exposure of NipR2F to peroxynitrite (E). MALDI MS Linear mode acquisition analyses demonstrate that both NipR2 and NipR2F peptides bind efficiently to intact human recombinant Rac1 (F).

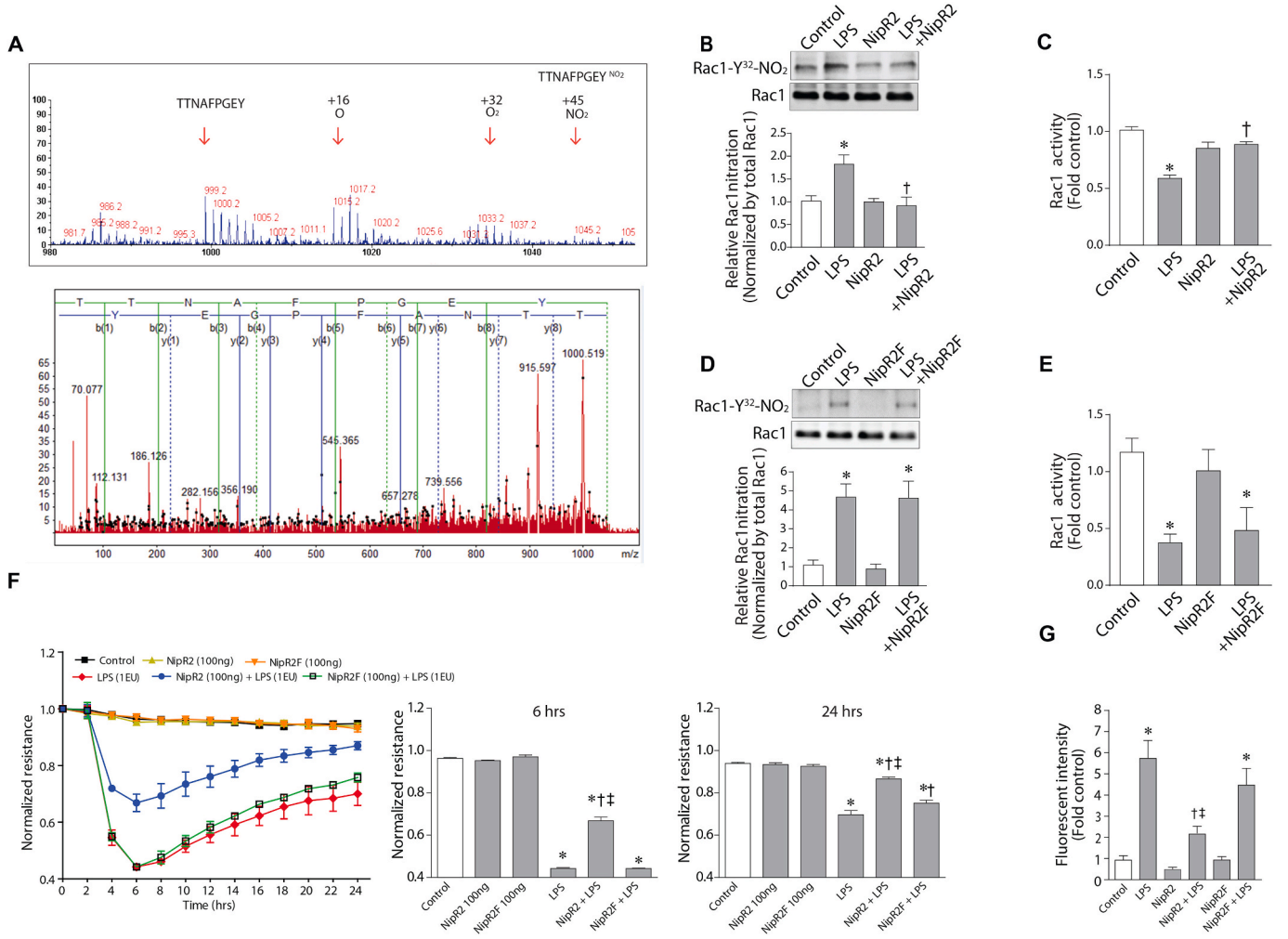

Fig. 5. The NipR2 peptide prevents LPS-mediated Rac1 nitration and preserves endothelial barrier function. HLMVEC were challenged with LPS (1 EU/ml, 4 h) and Rac1 protein was then immunoprecipitated and subjected to overnight in-gel chymotrypsin digestion. A nitrated peptide with sequence TTNAFPGEY^{32} was identified with a single nitration site present on the tyrosine residue and MALDI MS showed a typical photodecomposition pattern observed for addition of nitro group ([M+H]+, [M + H-16]+ and [M + H-32]+) (A). The MS/MS spectrum was fitted to the peptide sequence TTNAFPGEY from a human Rac1 protein modified at Tyr32 by nitro group (A). Cultured HLMVEC were pretreated with either NipR2 or NipR2F (5 μM, 5min) prior to LPS challenge (1 EU/ml, 4 h). Cells were harvested and lysates were subjected to Western blot analysis using the Rac1-Y^{32}-NO2 antibody. In the presence of NipR2 (B), but not NipR2F (D), the LPS-mediated increase in Rac1 protein nitration is attenuated. Similarly, the LPS-mediated inhibition of Rac1 GTPase activity is prevented by NipR2 (C), but not NipR2F (E). The decrease in TER in LPS challenged cells is attenuated by NipR2 but not NipR2F (F) with reductions in the nadir of TER (6 h post LPS challenge) and a stimulation of barrier restoration (24 h post LPS challenge). A representative normalized TER (fold change) trace from all groups is shown (F). Similarly, the LPS (1 EU/ml, 4 h) mediated extravasation of FITC-dextran was significantly attenuated in cells treated with NipR2 but not NipR2F (100 ng/ml) (G). NipR2 and NipR2F peptides were added at 100 ng/ml 30 min prior to LPS challenge. Data are mean ± SEM. N = 4. *P < 0.05 vs. Control; †P < 0.05 vs. LPS alone; ‡P < 0.05 vs. LPS + NipR2F.

[32]. Rac1 is involved in the maintenance and stabilization of microvascular endothelial barrier functions (maintains junctional formation and cell relaxation), whereas RhoA primarily acts antagonistically to impair barrier properties [33]. Post-translational modification can directly influence the structure, function and stability of the Rho GTPases [34]. This particular study confirms, for the first time, that Rac1 can be nitrated at Y^{32}, which leads to a persistent inhibition of GTPase activity. Crystal structure analysis of Rac1 indicates that Y^{32} lies adjacent to the nucleotide-binding site within the Switch I (residues 26–45), a region known to modulate GTP/GDP binding. The Switch regions in the Rac1 are the most important structural element of the protein. Molecular modeling analysis predicts that the nitration of Y^{32} of Rac1

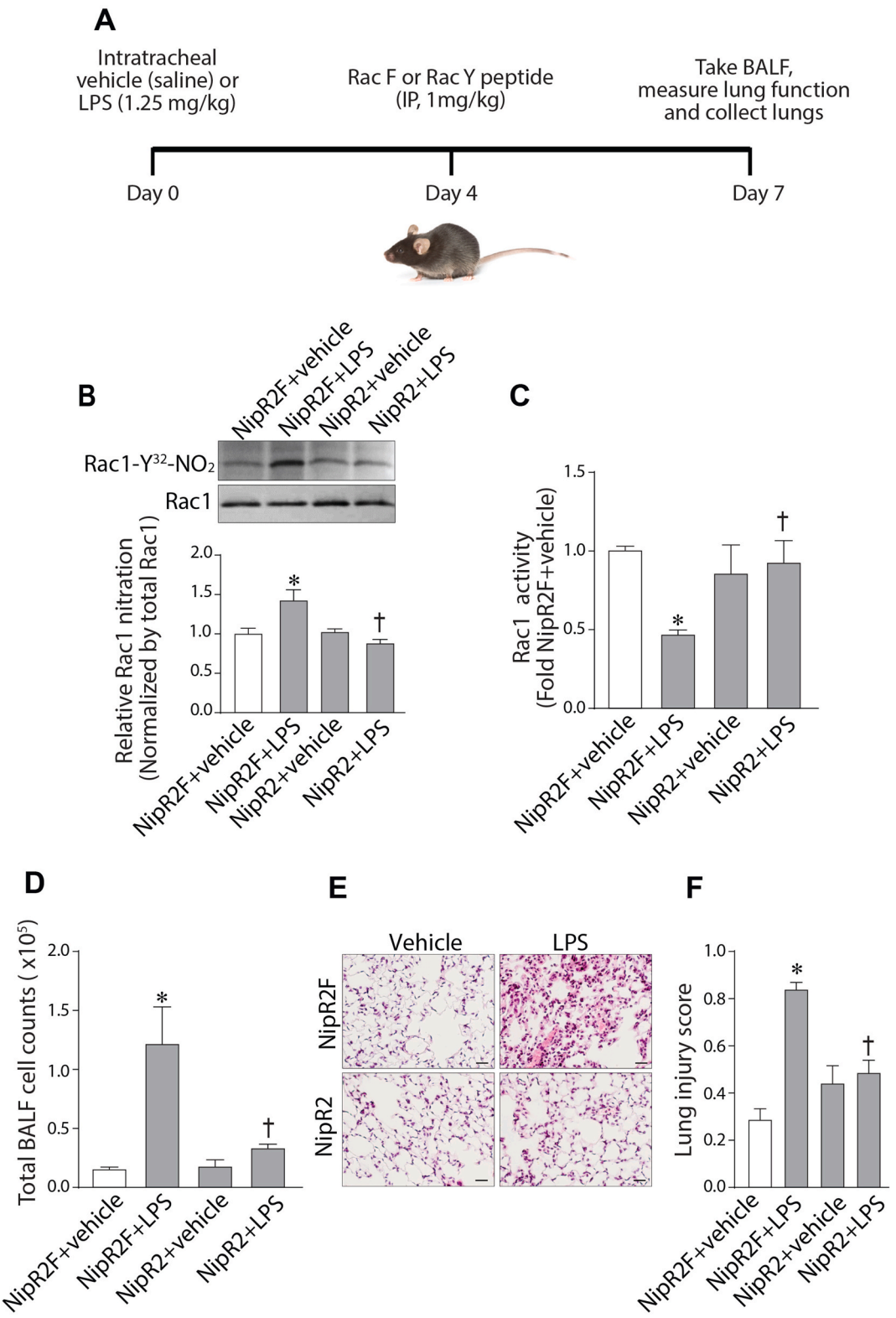

Fig. 6. The NipR2 peptide enhances lung repair after LPS exposure in the mouse. C57BI/6 mice received vehicle (0.9% saline) or LPS (1.25 mg/kg) prepared in 0.9% saline via an intratracheal injection 4 days before administration of NipR2 or NipR2F peptide (intraperitoneal injection, 1 mg/kg) (A). On Day 7 (post LPS) Rac1 nitration in lung protein homogenate was determined using Western blot analysis. In the presence of NipR2, but not NipR2F, the LPS-mediated increase in Rac1 protein nitration is reversed (B). Similarly, the LPS-mediated inhibition of Rac1 GTPase activity is reversed by NipR2, but not NipR2F (C). NipR2, but not NipR2F, also significantly attenuated the LPS-mediated increase in inflammatory cell numbers in the BALF on day 7 post-LPS (D). Lung sections were stained with hematoxylin and eosin (E, representative micrographs are shown) and scored for lung injury (F). NipR2, but not NipR2F, attenuated the lung injury score (F). Data are mean ± SEM. N = 4–6. *P < 0.05 vs. NipR2F + Vehicle; †P < 0.05 vs. NipR2F + LPS.

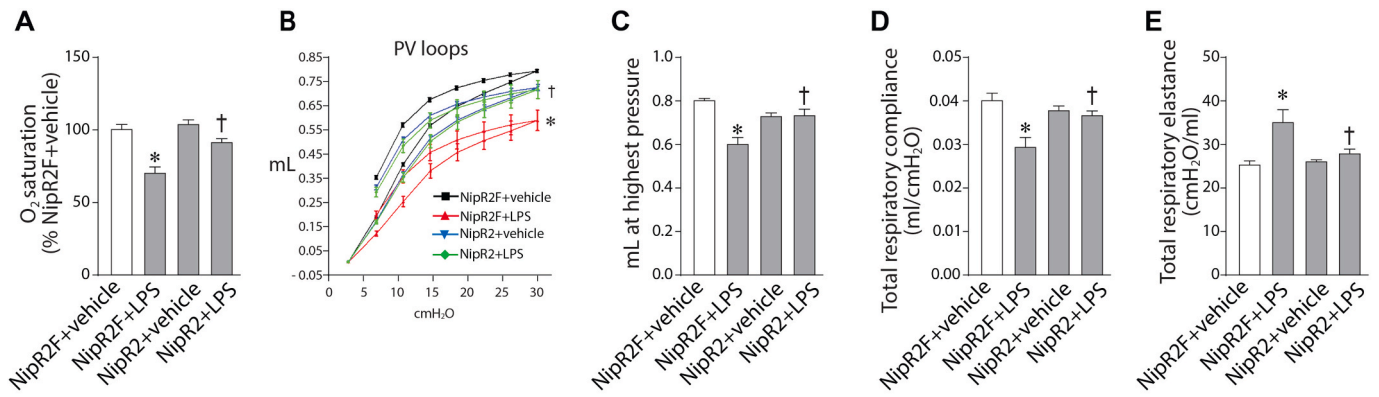

Fig. 7. NipR2 peptide restores lung function in mice exposed to LPS. C57BI/6 mice received vehicle (0.9% saline) or LPS (1.25 mg/kg) prepared in 0.9% saline via an intratracheal injection 4 days before administration of NipR2 or NipR2F peptide (intraperitoneal injection, 1 mg/kg) (A). On Day 7 (post LPS) Transcutaneous oxygen saturation was recorded using a small animal pulse oximeter. In the presence of NipR2, but not NipR2F, the LPS-mediated decrease in oxygen saturation is reversed (A). The analysis of dynamic pressure-volume relationships in the mouse lung also shows that NipR2, but not by NipR2F, reverses the LPS-mediated disruption of lung airway mechanics. The data represent pressure-volume loops for four groups with two curves, one for inhalation and one for exhalation events (B). The decrease in respiratory maximal volume at highest pressure (30 cmH_2O) is prevented by NipR2 (C). NipR2 also prevents the decrease in compliance (D). The increase in respiratory elastance is also attenuated by NipR2 (E). Data are mean ± SEM. N = 4–6. *P < 0.05 vs. NipR2F + Vehicle; †P < 0.05 vs. NipR2F + LPS.

preferentially stabilizes the closed conformation of Switch I. Comparing the Rac1 protein sequence to the RhoA protein reveals that there is an identical tyrosine residue (Y^{34} in RhoA and Y^{32} in Rac1) in the flexible flap region which is susceptible to nitration mediated modifications. The Rho GTPases share a conserved region for the nucleotide binding. The Switch I and Switch II regions are able to change their conformations when GDP is exchanged for GTP to signal downstream to effector proteins. Our prior work has demonstrated that nitration of Y^{34} in RhoA leads to the opening of the flap similar to that seen in the crystal structure containing a RhoA-GEF complex and that this decreases the affinity of RhoA for GDP, leading to faster GDP release, thus increasing RhoA activity [19]. In this study, our molecular dynamics simulations predict that peroxynitrite mediated nitration of Y^{32} in Rac1 leads to a closing of the flap region mimicking the conformational shift observed when a GDI is bound leading to decreased Rac1 GTPase activity. Another post translational modification of relevance is the S-nitrosylation of Ras superfamily GTPases. Nitric oxide (NO) can serve as important regulator of small GTPase proteins. NMR and X-ray crystal structures for Rho family GTPases propose that the Cys18 thiol in the GXXXXGK(S/T)C motif is accessible for solvent and suggest reactive oxygen species and reactive nitrogen species possibly target the Cys18 thiol [35–37]. Further, we have shown that S-nitrosylation of RhoA attenuates the activity of RhoA [38]. The effect of S-nitrosylation on Rac1 is unresolved but we speculate that as nitration activates while S-nitrosylation inhibits RhoA that S-nitrosylation may stimulate Rac1 activity. However, further studies will be required to test this possibility. Besides nitration a number of other post translational modifications have been reported that have the potential to alter its activity/function. These include ubiquitination [39–41], phosphorylation [42,43], and adenylylation (AMPylation) [44], all of which have all been shown to play important roles in the regulation of Rac1. Interestingly, it has been reported that Y^{32} in Rac1 is a target for AMPylation [44]. Therefore, we speculate that nitration might inhibit phosphorylation and/or AMPylation of Y^{32} in Rac1 which could permanently alter its activity. Thus, it is likely that the competition among these various potential modifications likely has both physiological and pathological implications. Again, further studies will be required to investigate this.

During sepsis-like conditions, LPS exposure stimulates the production of peroxynitrite which leads to protein nitration of tyrosine residues, a nonreversible event which often affects protein structure and function. Previously we had reported that peroxynitrite stress induced by LPS challenge causes RhoA nitration at Y^{34} which facilitates its persistent activation [19]. Rac1 and RhoA, as a balanced control mechanism of lung endothelial integrity, is disrupted by peroxynitrite stress. Even though RhoA and Rac1 share structural homology, RhoA is involved in endothelial barrier disruption during the development of ALI, while Rac1 is involved in endothelial barrier recovery during the resolution phase of ALI. The fact that each protein acts in a different phase of ALI could provide a therapeutic window to target Rac1, instead of RhoA, in the patients in ICU, most of whom have passed the earlier phase of endothelial disruption and are most likely in the slow recovery phase of this devastating disease. This possibility is supported by our animal studies in which we have utilized our NipR2 peptide to target Rac1 nitration in a "reversal"-, instead of "prevention"-, strategy to effectively "treat" experimental ALI. Our study reveals a new mechanism by which endothelial integrity loss is maintained through nitration-mediated Rac1 inhibition during sepsis-associated ALI. Importantly, we developed two new research tools in this study, a polyclonal antibody which specifically detects Y^{32}-nitrated Rac1, and NipR2, a synthetic peptide which prevents Rac1 nitration at Y^{32}. Since Rac1 is wildly expressed in multiple tissues with multidisciplinary function, our nitration specific Rac1 antibody has significant potential as a research tool in a number of pathologic states. Further, we validated the nitration shielding potency NipR2 in both cultured cells and a murine model of sepsis induced ALI. Thus, NipR2, or its next generation, may have clinical utility given the fact that ALI still does not have a selective drug therapy. However, this possibility should be tempered by the fact that previous ALI drug clinical trials have all failed. We propose that this is due to the fact that ALI is a syndrome that results from different insults (e.g., COVID-19 induced ALI is clearly different from trauma induced ALI), and the involvement of multiple systems failure such as endothelial barrier disruption, macrophage activation, and leukocyte infiltration. In this study, we report that NipR2 selectively targets Rac1 nitration and effectively blocks murine lung injury, but the therapeutic efficacy in ALI patients is hard to predict. We anticipate that a successful clinical efficacy of NipR2 or similar product might require: 1) precision medicine approach to identify patients in the sub-group with satisfactory responsiveness of Rac1 nitration blockade, as not all triggers of ALI (e.g., trauma) will lead to endothelial oxidative stress and peroxynitrite generation; 2) combination therapy with other effective reagents, including suppressor of the cytokine storm and/or neutrophil eliminators; 3) selective tissue delivery vehicle, to increase therapeutic index. Further, we propose that conditional genetically modified *in-vivo* models will be needed to fully elucidate the biological functions of the Rho GTPases in different physiological environments and pathological conditions, and this information will likely be required to develop

precise pharmacological inhibitors.

LPS is a known activator of endothelial ROS generation [45,46]. Interestingly the generation of ROS might be "designed" a result of detoxification of oxidative species in oxygen-rich environment, and sometimes as a signaling cascade, since it can be generated and removed quickly. However, these protective or regulatory signaling pathways can be overwhelmed, leading to "oxidative stress". In the lungs, multiple cell types, including endothelial cells, macrophages, epithelial cells, and infiltrated inflammatory leukocytes, are good ROS generators. LPS can activate several endogenous machineries to generate ROS including NADPH oxidase (NOX), uncoupled NOS, dysfunctional mitochondria, and xanthine oxidase, all of which have been reported to be involved with the oxidative stress associated with ALI [47–51]. The link between increased oxidative stress and lung injury, as well as the success of antioxidant therapy in preclinical models makes ROS generation an attractive target in ALI. However, the complex roles of ROS in ALI development and recovery have restricted the efficacy of antioxidant therapy. ROS is involved in tissue injury [52], barrier disruption [53], proinflammatory cytokine production [54]. While it is also involved in endothelial barrier recovery [55], and endothelial adherens junction re-assembly [56]. Endothelial cells have abundant NO which is mainly produced by eNOS, which, upon LPS-challenge mediated uncoupling, also starts to generate ROS. The downstream effector of NOS uncoupling is likely peroxynitrite, formed from the interaction of NO with superoxide generated from different sources. We propose that targeting adverse events downstream of ROS, such as Rac1 nitration, will be more selective and effective to terminate ROS associated adverse outcome, and reduce ALI. Nitration unlike phosphorylation, which is selectively mediated by kinases and phosphatases, and modulated by signaling cascades regulating these enzymes, is not dependent on enzymes to facilitate the post-translational modification. Peroxynitrite mediated tyrosine nitration is a covalent modification that adds a nitro group ($-NO_2$) to one ortho carbon of tyrosine's phenolic ring to form 3-nitrotyrosine. Protein tyrosine nitration introduces a net negative charge to the nitrated tyrosine at physiological pH, thus altering structural properties. Previously, we had reported that like Rac1, its antagomir RhoA can also be nitrated at Y^{34}, a similar location in the flexible flap region, leading to its persistent activation. We speculate that nitration will only occur at accessible tyrosine residues that are already sites for other post-translational modifications such as phosphorylation. Indeed, nitration is very similar to phosphorylation in terms of charge, and thus could lead to a similar structural/functional outcome to that obtained by phosphorylation. Alternatively, the presence of a 3-nitrotyrosine modification could potentially prevent the tyrosine residue being available for phosphorylation events. Since no enzyme has been identified as being responsible for the removal of nitration sites, mimicking the counter part of phosphatase for phosphorylation, the structure/function effect is persistent and thus deleterious as it is not balanced and countered. This might also explain the opposite functional outcome between Rac1 and RhoA nitration at a similar domain.

In conclusion, for the first time, we have used mass spectrometry as well as cell and molecular biology methodologies to identify Rac1 as being susceptible to nitration. This single nitration site located at Y^{32} leads to Rac1 GTPase inhibition and enhances LPS-mediated barrier disruption. We have also demonstrated that Rac1 nitration plays an important role in sepsis-mediated ALI and that blocking Rac1 nitration using a shielding peptide approach has therapeutic potential to reverse LPS-induced lung injury. Further studies will be required but this approach has the potential to produce a treatment for ALI that has so far proven to be intractable to all the pharmacologic approaches tried to date.

Declaration of competing interest

The authors have no conflict of interest to declare related to this research article.

Acknowledgements

This work was supported in part by HL60190 , (SMB), HL137282 (SMB), HL134610 (SMB and TW), HL146369 (SMB and TW), R01HL142212 (SMB), and the Interdisciplinary Training in Cardiovascular Research T32 HL007249 (to XW) all from the National Heart, Lung, and Blood Institute, Bethesda, MD USA.

Appendix A. Supplementary data

Supplementary data to this article can be found online at https://doi.org/10.1016/j.redox.2020.101794.

His-tagged human Rac1 recombinant protein was purified from *E. coli* BL21 strain using a Hisprep FF 16/10 column and further separated by size-exclusion chromatography. Purity was confirmed by SDS-PAGE followed by Coomassie Blue staining (A) and Western blot analysis using a Rac1 specific antibody (B). Recombinant Rac1 protein was incubated or not with authentic peroxynitrite (100 μM, 30 min), and the chymotrypsin digested Rac1 peptides were subjected to MALDI-TOF MS and MS/MS analysis. A single nitrated peptide with sequence TTNAFPGEY* was identified in peroxynitrite incubated Rac1 protein sample corresponding to a peptide mass of 1044.4 *m/z* from its unnitrated mass of 999.4 *m/z*. Further, MS/MS analysis of the 1044.4 *m/z* peptide was obtained in positive reflector mode (C). The resulting MS/MS spectrum was fitted to the peptide sequence ($TTNAFPGEY^{NO}{}_2$) from human Rac1 protein (C). A Rac1-HIS adenoviral construct was used to transduce PAEC (48 h, MOI = 5) and the Rac1-HIS protein was purified using a HisPur Ni-NTA Column. Samples (control cell lysate, transduced cell lysate, and purified Rac1) were separated by SDS-PAGE and stained with Coomassie blue dye (D) or subjected to Western blot analysis using Rac1 antibody (E). PAEC transduced with Rac1-HIS adenovirus were then exposed to SIN-1 (200 μM, 1 h) and Western blot analysis confirmed equal Rac1 protein levels between untreated and SIN-1 treated PAEC (F) and a strong band was observed at 21.5 kDa after probing with nitrotyrosine antibody indicating SIN-1 mediated Rac1 nitration in PAEC (G). Reprobing with an antibody to β-actin was used to verify equal loading (F&G). Human Rac1-HIS protein was digested with chymotrypsin and the Rac1 peptides subjected to MALDI-TOF MS and MS/MS analysis. Rac1 protein isolated from endothelial cells treated with SIN-1 exhibited the same nitration site on Y^{32} ($TTNAFPGEY^{NO}{}_2$) on human Rac1 (H). Molecular dynamic simulations of Rac1 nitrated at Y^{32} within the flexible region (flap) of the Switch I domain responsible for nucleotide binding was carried out and the movement of the flap region was superimposed onto the X-ray crystal structure Rac1 protein demonstrating a more closed configuration when Y^{32} is nitrated (I). Molecular dynamic simulations of the flap region in RhoA nitrated at Y^{34} was carried out and the movement of the flap region was superimposed onto the X-ray crystal structure RhoA protein demonstrating a more open configuration when Y^{34} is nitrated (J).

A polyclonal antibody was generated to selectively detect the Rac1 protein when nitrated at Y^{32} (Rac1-Y^{32}-NO2). To test its specificity, Western blot analysis was carried out on His-tagged human Rac1 recombinant protein purified by a Ni-NTA column incubated or not with authentic peroxynitrite (100 μM, 30 min) (A) or HLMVEC exposed to SIN-1 (200 μM, 1 h) (B). Both peroxynitrite (A) and SIN-1 (B) increased the levels of nitrated Rac1 observed in *in-vitro* and *in-vivo* experiments respectively. Reprobing with an antibody to β-actin was used to verify equal loading (B). Purified human recombinant Rac1 or RhoA [19] were exposed or not to the peroxynitrite donor, SIN-1 (100 μM, 15min) then subjected to Western blot analysis using custom made antibodies specific to either nitrated Rac1 or nitrated RhoA (C). There is increased binding with the Rac1-Y^{32}-NO_2 and RhoA-Y^{34}-NO2 antibodies to their cognitive proteins after SIN-1 exposure (C). C57/B6 mice were challenged with LPS (i.t. 6.75×10^4 Endotoxin Units/g body weight, 12 h) in the presence or absence of MnTMPyP (i.p. 5 mg/kg body weight). Lung tissues were harvested and lysates subjected to Western blot analysis

using the Rac1-Y^{32}-NO2 antibody. LPS exposure increases Rac1 nitration in the mouse lung and this is attenuated in the presence of MnTMPyP (D). Membranes were reprobed with Rac1 to normalize for total Rac1 levels (D). Rac 1 GTPase activity is also inhibited by LPS and preserved in the presence of MnTMPyP (E). Data are mean ± SEM. N = 4. *P < 0.05 vs. Control; †P < 0.05 vs. LPS alone.

References

[1] X. Li, X. Ma, Acute respiratory failure in COVID-19: is it "typical" ARDS? Crit. Care 24 (1) (2020) 198, https://doi.org/10.1186/s13054-020-02911-9, 2020.

[2] E. Roupie, E. Lepage, M. Wysocki, J.Y. Fagon, J. Chastre, D. Dreyfuss, H. Mentec, J. Carlet, C. Brun-Buisson, F. Lemaire, L. Brochard, Prevalence, etiologies and outcome of the acute respiratory distress syndrome among hypoxemic ventilated patients. SRLF Collaborative Group on Mechanical Ventilation, Société de Réanimation de Langue Française, Intensive Care Med 25 (9) (1999) 920–929.

[3] T. Yoshida, Y. Fujino, M.B. Amato, B.P. Kavanagh, Fifty years of research in ARDS. Spontaneous breathing during mechanical ventilation. Risks, mechanisms, and management, Am. J. Respir. Crit. Care Med. 195 (8) (2017) 985–992.

[4] T.A. Dernaika, J.I. Keddissi, G.T. Kinasewitz, Update on ARDS: beyond the low tidal volume, Am. J. Med. Sci. 337 (5) (2009) 360–367.

[5] K. Buttenschoen, M. Kornmann, D. Berger, G. Leder, H.G. Beger, C. Vasilescu, Endotoxemia and endotoxin tolerance in patients with ARDS, Langenbeck's Arch. Surg. 393 (4) (2008) 473–478.

[6] A. Daiber, S. Chlopicki, Revisiting pharmacology of oxidative stress and endothelial dysfunction in cardiovascular disease: evidence for redox-based therapies, Free Radic. Biol. Med. 1 (19) (2020) 31702, 2.

[7] T.M. Wizemann, C.R. Gardner, J.D. Laskin, S. Quinones, S.K. Durham, N.L. Goller, S.T. Ohnishi, D.L. Laskin, Production of nitric oxide and peroxynitrite in the lung during acute endotoxemia, J. Leukoc. Biol. 56 (6) (1994) 759–768.

[8] S. Sharma, A. Smith, S. Kumar, S. Aggarwal, I. Rehmani, C. Snead, C. Harmon, J. Fineman, D. Fulton, J.D. Catravas, S.M. Black, Mechanisms of nitric oxide synthase uncoupling in endotoxin-induced acute lung injury: role of asymmetric dimethylarginine, Vasc. Pharmacol. 52 (5–6) (2010) 182–190.

[9] H. Ischiropoulos, L. Zhu, J. Chen, M. Tsai, J.C. Martin, C.D. Smith, J.S. Beckman, Peroxynitrite-mediated tyrosine nitration catalyzed by superoxide dismutase, Arch. Biochem. Biophys. 298 (2) (1992) 431–437.

[10] P.F. Good, A. Hsu, P. Werner, D.P. Perl, C.W. Olanow, Protein nitration in Parkinson's disease, J. Neuropathol. Exp. Neurol. 57 (4) (1998) 338–342.

[11] K. Ckless, A. Lampert, J. Reiss, D. Kasahara, M.E. Poynter, C.G. Irvin, L. K. Lundblad, R. Norton, A. van der Vliet, Y.M. Janssen-Heininger, Inhibition of arginase activity enhances inflammation in mice with allergic airway disease, in association with increases in protein S-nitrosylation and tyrosine nitration, J. Immunol. 181 (6) (2008) 4255–4264.

[12] G. Guilgen, M.L. Werneck, L. de Noronha, A.P. Martins, A.M. Varela, L.S. Nakao, R. Pecoits-Filho, Increased calcification and protein nitration in arteries of chronic kidney disease patients, Blood Purif. 32 (4) (2011) 296–302.

[13] H. Sugiura, M. Ichinose, M. Tomaki, H. Ogawa, A. Koarai, T. Kitamuro, Y. Komaki, T. Akita, H. Nishino, S. Okamoto, T. Akaike, T. Hattori, Quantitative assessment of protein-bound tyrosine nitration in airway secretions from patients with inflammatory airway disease, Free Radic. Res. 38 (1) (2004) 49–57.

[14] S.M. Dudek, J.G. Garcia, Cytoskeletal regulation of pulmonary vascular permeability, J. Appl. Physiol. 91 (4) (1985) 1487–1500.

[15] M. Bruewer, A.M. Hopkins, M.E. Hobert, A. Nusrat, J.L. Madara, RhoA, Rac1, and Cdc42 exert distinct effects on epithelial barrier via selective structural and biochemical modulation of junctional proteins and F-actin, Am. J. Physiol. Cell Physiol. 287 (2) (2004) C327–C335.

[16] B. Wójciak-Stothard, S. Potempa, T. Eichholtz, A.J. Ridley, Rho and Rac but not Cdc42 regulate endothelial cell permeability, J. Cell Sci. 114 (Pt 7) (2001) 1343–1355.

[17] F. Huang, P.V. Subbaiah, O. Holian, J. Zhang, A. Johnson, N. Gertzberg, H. Lum, Lysophosphatidylcholine increases endothelial permeability: role of PKCalpha and RhoA cross talk, Am. J. Physiol. Lung Cell Mol. Physiol. 289 (2) (2005) L176–L185.

[18] Z.M. Goeckeler, R.B. Wysolmerski, Myosin phosphatase and cofilin mediate cAMP/cAMP-dependent protein kinase-induced decline in endothelial cell isometric tension and myosin II regulatory light chain phosphorylation, J. Biol. Chem. 280 (38) (2005) 33083–33095.

[19] R. Rafikov, C. Dimitropoulou, S. Aggarwal, A. Kangath, C. Gross, D. Pardo, S. Sharma, A. Jezierska-Drutel, V. Patel, C. Snead, R. Lucas, A. Verin, D. Fulton, J. D. Catravas, S.M. Black, Lipopolysaccharide-induced lung injury involves the nitration-mediated activation of RhoA, J. Biol. Chem. 289 (8) (2014) 4710–4722.

[20] J.D. Catravas, C. Snead, C. Dimitropoulou, A.S. Chang, R. Lucas, A.D. Verin, S. M. Black, Harvesting, Identification and barrier function of human lung microvascular endothelial cells, Vasc. Pharmacol. 52 (5–6) (2010) 175–181.

[21] N. Sud, S. Sharma, D.A. Wiseman, C. Harmon, S. Kumar, R.C. Venema, J. R. Fineman, S.M. Black, Nitric oxide and superoxide generation from endothelial NOS: modulation by HSP90, Am. J. Physiol. Lung Cell Mol. Physiol. 293 (6) (2007) L1444–L1453.

[22] S. Sharma, N. Sud, D.A. Wiseman, A.L. Carter, S. Kumar, Y. Hou, T. Rau, J. Wilham, C. Harmon, P. Oishi, J.R. Fineman, S.M. Black, Altered carnitine homeostasis is associated with decreased mitochondrial function and altered nitric oxide signaling in lambs with pulmonary hypertension, Am. J. Physiol. Lung Cell Mol. Physiol. 294 (1) (2008) L46–L56.

[23] S. Aggarwal, C.M. Gross, R. Rafikov, S. Kumar, J.R. Fineman, B. Ludewig, D. Jonigk, S.M. Black, Nitration of tyrosine 247 inhibits protein kinase G-1α activity by attenuating cyclic guanosine monophosphate binding, J. Biol. Chem. 289 (11) (2014) 7948–7961.

[24] C.M. Gross, R. Rafikov, S. Kumar, S. Aggarwal, P.B. Ham 3rd, M.L. Meadows, M. Cherian-Shaw, A. Kangath, S. Sridhar, R. Lucas, S.M. Black, Endothelial nitric oxide synthase deficient mice are protected from lipopolysaccharide induced acute lung injury, PloS One 10 (3) (2015).

[25] S.M. Black, M.J. Johengen, Z.D. Ma, J. Bristow, S.J. Soifer, Ventilation and oxygenation induce endothelial nitric oxide synthase gene expression in the lungs of fetal lambs, J. Clin. Invest. 100 (6) (1997) 1448–1458.

[26] T. Wang, E.T. Chiang, L. Moreno-Vinasco, G.D. Lang, S. Pendyala, J.M. Samet, A. S. Geyh, P.N. Breysse, S.N. Chillrud, V. Natarajan, J.G. Garcia, Particulate matter disrupts human lung endothelial barrier integrity via ROS- and p38 MAPK-dependent pathways, Am. J. Respir. Cell Mol. Biol. 42 (4) (2010) 442–449.

[27] G. Matute-Bello, G. Downey, B.B. Moore, S.D. Groshong, M.A. Matthay, A. S. Slutsky, W.M. Kuebler, An official American Thoracic Society workshop report: features and measurements of experimental acute lung injury in animals, Am. J. Respir. Cell Mol. Biol. 44 (5) (2011) 725–738.

[28] S. Aggarwal, C.M. Gross, S. Kumar, C. Dimitropoulou, S. Sharma, B.A. Gorshkov, S. Sridhar, Q. Lu, N.V. Bogatcheva, A.J. Jezierska-Drutel, R. Lucas, A.D. Verin, J. D. Catravas, S.M. Black, Dimethylarginine dimethylaminohydrolase II overexpression attenuates LPS-mediated lung leak in acute lung injury, Am. J. Respir. Cell Mol. Biol. 50 (3) (2014) 614–625.

[29] H. Ohta, S. Chiba, M. Ebina, M. Furuse, T. Nukiwa, Altered expression of tight junction molecules in alveolar septa in lung injury and fibrosis, Am. J. Physiol. Lung Cell Mol. Physiol. 302 (2) (2012) 14.

[30] E.S. Harris, W.J. Nelson, VE-cadherin: at the front, center, and sides of endothelial cell organization and function, Curr. Opin. Cell Biol. 22 (5) (2010) 651–658.

[31] V. Spindler, N. Schlegel, J. Waschke, Role of GTPases in control of microvascular permeability, Cardiovasc. Res. 87 (2) (2010) 243–253.

[32] B. Wojciak-Stothard, A.J. Ridley, Rho GTPases and the regulation of endothelial permeability, Vasc. Pharmacol. 39 (4–5) (2002) 187–199.

[33] L.K. Nguyen, B.N. Kholodenko, A. von Kriegsheim, Rac1 and RhoA: networks, loops and bistability, Small GTPases 9 (4) (2018) 316–321.

[34] M.F. Olson, Rho GTPases, their post-translational modifications, disease-associated mutations and pharmacological inhibitors, Small GTPases 9 (3) (2018) 203–215.

[35] K. Ihara, S. Muraguchi, M. Kato, T. Shimizu, M. Shirakawa, S. Kuroda, K. Kaibuchi, T. Hakoshima, Crystal structure of human RhoA in a dominantly active form complexed with a GTP analogue, J. Biol. Chem. 273 (16) (1998) 9656–9666.

[36] M. Hirshberg, R.W. Stockley, G. Dodson, M.R. Webb, The crystal structure of human rac1, a member of the rho-family complexed with a GTP analogue, Nat. Struct. Biol. 4 (2) (1997) 147–152.

[37] B.S. Zuckerbraun, D.A. Stoyanovsky, R. Sengupta, R.A. Shapiro, B.A. Ozanich, J. Rao, J.E. Barbato, E. Tzeng, Nitric oxide-induced inhibition of smooth muscle cell proliferation involves S-nitrosation and inactivation of RhoA, Am. J. Physiol. Cell Physiol. 292 (2) (2007) 16.

[38] F. Chen, Y. Wang, R. Rafikov, S. Haigh, W.B. Zhi, S. Kumar, P.T. Doulias, O. Rafikova, H. Pillich, T. Chakraborty, R. Lucas, A.D. Verin, J.D. Catravas, J. X. She, S.M. Black, D.J.R. Fulton, RhoA S-nitrosylation as a regulatory mechanism influencing endothelial barrier function in response to G(+)-bacterial toxins, Biochem. Pharmacol. 127 (2017) 34–45.

[39] S. Castillo-Lluva, C.T. Tan, M. Daugaard, P.H. Sorensen, A. Malliri, The tumour suppressor HACE1 controls cell migration by regulating Rac1 degradation, Oncogene 32 (13) (2013) 1735–1742.

[40] T.K. Oberoi, T. Dogan, J.C. Hocking, R.P. Scholz, J. Mooz, C.L. Anderson, C. Karreman, D. Meyer zu Heringdorf, G. Schmidt, M. Ruonala, K. Namikawa, G. S. Harms, A. Carpy, B. Macek, R.W. Köster, K. Rajalingam, IAPs regulate the plasticity of cell migration by directly targeting Rac1 for degradation, EMBO J. 31 (1) (2012) 14–28.

[41] J. Zhao, R.K. Mialki, J. Wei, T.A. Coon, C. Zou, B.B. Chen, R.K. Mallampalli, Y. Zhao, SCF E3 ligase F-box protein complex SCF(FBXL19) regulates cell migration by mediating Rac1 ubiquitination and degradation, Faseb. J. 27 (7) (2013) 2611–2619.

[42] F. Chang, C. Lemmon, D. Lietha, M. Eck, L. Romer, Tyrosine phosphorylation of Rac1: a role in regulation of cell spreading, PloS One 6 (12) (2011) 6.

[43] T. Kwon, D.Y. Kwon, J. Chun, J.H. Kim, S.S. Kang, Akt protein kinase inhibits Rac1-GTP binding through phosphorylation at serine 71 of Rac1, J. Biol. Chem. 275 (1) (2000) 423–428.

[44] C.A. Worby, S. Mattoo, R.P. Kruger, L.B. Corbeil, A. Koller, J.C. Mendez, B. Zekarias, C. Lazar, J.E. Dixon, The fic domain: regulation of cell signaling by adenylylation, Mol Cell 34 (1) (2009) 93–103.

[45] U. Maitra, N. Singh, L. Gan, L. Ringwood, L. Li, IRAK-1 contributes to lipopolysaccharide-induced reactive oxygen species generation in macrophages by inducing NOX-1 transcription and Rac1 activation and suppressing the expression of antioxidative enzymes, J. Biol. Chem. 284 (51) (2009) 35403–35411.

[46] K. Sato, M.B. Kadiiska, A.J. Ghio, J. Corbett, Y.C. Fann, S.M. Holland, R. G. Thurman, R.P. Mason, In vivo lipid-derived free radical formation by NADPH oxidase in acute lung injury induced by lipopolysaccharide: a model for ARDS, Faseb. J. 16 (13) (2002) 1713–1720.

[47] E. Kratzer, Y. Tian, N. Sarich, T. Wu, A. Meliton, A. Leff, A.A. Birukova, Oxidative stress contributes to lung injury and barrier dysfunction via microtubule destabilization, Am. J. Respir. Cell Mol. Biol. 47 (5) (2012) 688–697.

[48] H.S. Park, J.N. Chun, H.Y. Jung, C. Choi, Y.S. Bae, Role of NADPH oxidase 4 in lipopolysaccharide-induced proinflammatory responses by human aortic endothelial cells, Cardiovasc. Res. 72 (3) (2006) 447–455.

[49] S. Sharma, A. Smith, S. Kumar, S. Aggarwal, I. Rehmani, C. Snead, C. Harmon, J. Fineman, D. Fulton, J.D. Catravas, S.M. Black, Mechanisms of nitric oxide synthase uncoupling in endotoxin-induced acute lung injury: role of asymmetric dimethylarginine, Vasc. Pharmacol. 52 (5) (2010) 182–190.
[50] M. Vuda, M. Chiusa, S.M. Jakob, J. Takala, C. Zuppinger, S. Djafarzadeh, Lipopolysaccharide induces mitochondrial dysfunction in rat cardiac microvascular endothelial cells, Crit. Care 15 (1) (2011) P245.
[51] P.M. Hassoun, F.S. Yu, C.G. Cote, J.J. Zulueta, R. Sawhney, K.A. Skinner, H. B. Skinner, D.A. Parks, J.J. Lanzillo, Upregulation of xanthine oxidase by lipopolysaccharide, interleukin-1, and hypoxia. Role in acute lung injury, Am. J. Respir. Crit. Care Med. 158 (1) (1998) 299–305.
[52] M. Kellner, S. Noonepalle, Q. Lu, A. Srivastava, E. Zemskov, S.M. Black, ROS signaling in the pathogenesis of acute lung injury (ALI) and acute respiratory distress syndrome (ARDS), Adv. Exp. Med. Biol. 967 (2017) 105–137.
[53] D. Zhang, J. Zhou, L.C. Ye, J. Li, Z. Wu, Y. Li, C. Li, Autophagy maintains the integrity of endothelial barrier in LPS-induced lung injury, J. Cell. Physiol. 233 (1) (2018) 688–698.
[54] M.M. Ndengele, C. Muscoli, Z.Q. Wang, T.M. Doyle, G.M. Matuschak, D. Salvemini, Superoxide potentiates NF-kappaB activation and modulates endotoxin-induced cytokine production in alveolar macrophages, Shock 23 (2) (2005) 186–193.
[55] A. Boueiz, P.M. Hassoun, Regulation of endothelial barrier function by reactive oxygen and nitrogen species, Microvasc. Res. 77 (1) (2009) 26–34.
[56] S. van Wetering, J.D. van Buul, S. Quik, F.P.J. Mul, E.C. Anthony, J.-P.t. Klooster, J. G. Collard, P.L. Hordijk, Reactive oxygen species mediate Rac-induced loss of cell-cell adhesion in primary human endothelial cells, J. Cell Sci. 115 (9) (2002) 1837–1846.